THESIS FOR THE DEGREE OF LICENTIATE OF
ENGINEERING
IN
THERMO AND FLUID DYNAMICS

CFD Modeling of Combustion in Flexi-Fuel Burners at Gas Turbine Conditions

ABDALLAH ABOU-TAOUK

Division of Fluid Dynamics

Department of Applied Mechanics

CHALMERS UNIVERSITY OF TECHNOLOGY

Göteborg, Sweden, 2011

CFD Modeling of Combustion in Flexi-Fuel Burners at Gas Turbine Conditions

ABDALLAH ABOU-TAOUK

Thesis for Licentiate of Engineering no. 2011:10
ISSN 1652-8565

Division of Fluid Dynamics
Department of Applied Mechanics
Chalmers University of Technology
SE-412 96 Göteborg, Sweden

Phone: +46-(0)31-7721400
Fax: +46-(0)31-180976

Printed at Chalmers Reproservice
Göteborg, Sweden, 2011

CFD Modeling of Combustion in Flexi-Fuel Burners at Gas Turbine Conditions

ABDALLAH ABOU-TAOUK

Division of Fluid Dynamics
Department of Applied Mechanics
Chalmers University of Technology

Abstract

The main source of energy in the nearest future will come from fossil fuels. Increasing demands on environmentally friendly energy conversion implies that pollutants, such as CO and NO_x, need to be reduced.

This project aims to investigate recent developments in combustion modeling and turbulence modeling in the context of engineering type Computational Fluid Dynamics (CFD) analysis tools, applied to the main problem area of swirl-stabilized flexi-fuel flames. To perform a CFD simulation of reacting flows, kinetic information needs to be provided to the CFD code. Fully detailed kinetic mechanisms are expensive in terms of computer time when coupled with CFD and hence the use of global reaction mechanisms is preferable. Global mechanisms consist of a reduced number of reactions mostly one-way reactions which are governed by tuned Arrhenius rate expressions. The optimization at each equivalence ratio is here done by comparing results from Perfectly Stirred Reactor (PSR) calculations for both a detailed reference mechanism and the chosen multi-step global reaction mechanisms.

Steady-state Reynolds Averaged Navier Stokes (RANS), hybrid Unsteady RANS/Large Eddy Simulation (URANS/LES) and LES turbulence models have been used in the CFD work. This thesis includes the development and derivation of new 3-step global reaction mechanism for methane-air flames, which has been implemented and evaluated in the CFD analysis for two different burner configurations. In papers I and II an atmospheric burner test rig at Lund University (LTH) has been modeled and the results have been compared to high quality experimental data (emission and Particle Image Velocimetry (PIV) data). There is good agreement between the CFD simulations and measurements of emissions, velocity field and flame visualization. The second configuration that has been modeled and compared with experimental data is the Sandia Flame D test case, which is reported in paper III.

Keywords: CFD, Chemistry, Combustion, RANS, LES, SAS-SST, PSR, Global reaction mechanism

List of Publications

This thesis is based on the work contained in the following papers:

I Abdallah Abou-Taouk and Lars-Erik Eriksson , 2011, Optimized Global Mechanisms For CFD Analysis Of Swirl-Stabilized Syngas Burner For Gas Turbines, *ASME Turbo Expo 2011*, June 6-11, Vancouver, Canada

II Abdallah Abou-Taouk, Ronald Whiddon, Ivan R. Sigfrid and Lars-Erik Eriksson , 2011, CFD Investigation Of Swirl-Stabilized Flexi-Fuel Burner Using Methane-Air Mixture For Gas Turbines, 2011, *20th International Society for Airbreathing Engines*, ISABE 2011-1122, September 12-16, Gothenburg, Sweden

III Abdallah Abou-Taouk and Lars-Erik Eriksson, Evaluation of Optimized 3-step Global Reaction Mechanism for CFD Simulations on Sandia Flame D , 2011, *The 6th Symposium on Numerical Analysis of Fluid Flow and Heat Transfer*, ICNAAM 2011-0604, September 18-25, Halkidiki, Greece

Acknowledgments

This work was carried out at the Department of Applied Mechanics, Division of Fluid Dynamics at Chalmers University of Technology. This research has been funded by the Swedish Energy Agency, Siemens Industrial Turbomachinery AB, Volvo Aero Corporation, and the Royal Institute of Technology through the Swedish research program TURBOPOWER, the support of which is gratefully acknowledged.

First and foremost, I would like to express my highly appreciate to my supervisor Prof. Lars-Erik Eriksson for his great guidance and support, sharing his knowledge and ideas with me. I would also like to thank my colleagues and friends at the Division of Fluid Dynamics and especially Ph.D students Lars Ellbrant and Mohamad El-Alti, for all the invaluable help and pleasant discussions with me. The administrative support by Ulla Lindberg-Thieme and Monica Vargman is gratefully acknowledged.

Specially thanks to Dr. Jenny Larfeldt and Dr. Darioush Gohari Barhaghi at Siemens Industrial Turbomachinery AB in Finspång. I appreciate the helpful discussions we had and sharing the geometry with me. I would also thank the Ph.D students Ivan Sigfrid and Ronald Whiddon at Lund University for providing the experimental data.

The CFD simulations were performed on C3SE computing resources. Thomas Svedberg at C3SE is acknowledged for his assistance concerning technical aspects and implementation in making the Ansys CFX code run on the C3SE resources.

Finally, my warmest gratitude goes to my father, my mother, my four sisters, my wife Douaa and my wonderful two daughters Sabah and Laila. The work could never have been done without the support and encouragement from you.

Nomenclature

Upper-case Roman

A	pre-exponential factor
B_k	backward reaction rate
C_μ	constant in k-ε turbulence model
E_a	activation energy
F_k	forward reaction rate
$[I]$	molar concentration
K_c	equilibrium constant
$L_{\nu k}$	von karman length scale
P_{in}	inlet reactor pressure
P_k	turbulent production term
RR	reaction rate
S_{ij}	strain rate tensor
S_L	laminar flame speed
S_{SAS}	source term in SAS model
S	swirl number
T	temperature
T_{in}	inlet reactor temperature
T_{out}	outlet reactor temperature
V	reactor volume
Y	mass fraction
$Y^{(k)}$	species mass fraction

Lower-case Roman

f_1	correction function
f_2	correction function
h_0	total enthalpy
k	kinetic energy
$\dot{m}$	mass flow rate
p	pressure
u_i	cartesian components of velocity vector

u	axial velocity component
v	radial velocity component
w	tangential velocity component

Greek Symbols

ϕ	equivalence ratio
β	temperature exponent
$\beta^\star$	constant in k-ω turbulence model
δ_{ij}	kronecker delta
ε	dissipation of turbulent kinetic energy
μ	laminar dynamic viscosity
μ_t	turbulent eddy viscosity
ν	kinematic viscosity ($\nu = \mu/\rho$)
ρ	density
τ_{ij}	viscous stress tensor
τ_{res}	residence time

Abbreviations

CFD	Computational Fluid Dynamics
CFL	Courant-Friedrichs-Lewy
DES	Detached Eddy Simulation
DLE	Dry Low Emission
DNS	Direct Numerical Simulation
EDM	Eddy Dissipation Model
FRC	Finite Rate Chemistry
LCV	Low Caloric Value
LDV	Laser Doppler Velocimetry
LES	Large Eddy Simulation
LTH	Lund University
MFL	Mass Flow Controllers
M3	Meredith 3-step reaction mechanism
PIV	Particle Image Velocimetry
PLIF	Planar Laser-Induced Fluorescence Imaging
PSR	Perfectly Stirred Reactor
RANS	Reynolds Averaged Navier-Stokes
RPL	Rich Pilot Lean
RNG	Re-Normalisation Group
SAS	Scale Adaptive Simulation
SCADA	Supervisory Control Data Acquisition
SIT	Siemens Industrial Turbomachinery
UHC	Unburned HydroCarbons

URANS	Unsteady Reynolds Averaged Navier-Stokes
WALE	Wall Adaptive Local Eddy Viscosity
WD2	Westbrook Dryer 2-step reaction mechanism

Chemical Compunds

CO_2	carbon dioxide
CO	carbon monoxide
H_2	hydrogen
CH_4	methane
NO_x	nitrogen oxides
O_2	oxygen

Contents

Abstract iii

List of Publications v

Acknowledgments vii

Nomenclature ix

1 Introduction 1
- 1.1 Motivation . . . 1
- 1.2 Kinetic Modeling . . . 3
- 1.3 Turbulence-Chemistry Interaction . . . 3
- 1.4 Turbulence Modeling . . . 4
- 1.5 The Flexi-Fuel Burner . . . 5
- 1.6 Experimental Setup . . . 6

2 Kinetics 7
- 2.1 Global Reaction Mechanisms . . . 7
- 2.2 The Perfectly Stirred Reactor Model . . . 9
- 2.3 Optimization Strategy . . . 10
  - 2.3.1 Methane-Air Mixture . . . 10
  - 2.3.2 Syngas Mixture . . . 11
- 2.4 Results of the Kinetic Optimization . . . 12
- 2.5 Flame Speed . . . 14

3 Combustion and CFD 15
- 3.1 Turbulent Combustion . . . 15
- 3.2 FRC Model . . . 15
- 3.3 EDM Model . . . 16

4 Geometry and Mesh 17
- 4.1 The SGT 750 Engine . . . 17
- 4.2 CFD-Model of the Scaled Flexi-Fuel Burner . . . 18
- 4.3 Hexahedral Meshing . . . 19

5 Numerical Method and Turbulence Modeling **23**
5.1 Introduction 23
5.2 Governing Equations 23
5.3 $k-\omega$ SST 24
5.4 RNG $k-\epsilon$ 24
5.5 SAS-SST 25

6 CFD Results **27**
6.1 Boundary Conditions 27
6.2 Swirl Number 28
6.3 SAS-SST Results 28
6.3.1 Flow Field 28
6.3.2 Temperature 30
6.4 LES-WALE Results 30

7 Summary of Papers **33**
7.1 Paper I 33
7.1.1 Motivation and Work 33
7.1.2 Results 33
7.2 Paper II 34
7.2.1 Motivation and Work 34
7.2.2 Results 34
7.3 Paper III 34
7.3.1 Motivation and Work 34
7.3.2 Results 34

8 Concluding Remarks **35**

Bibliography **37**

Chapter 1

Introduction

1.1 Motivation

Today, nuclear power, biomass energy and other renewable energy accounts for approximately 20% of the total energy consumption in the world. This implies that combustion of fossil fuels will remain the dominating energy conversion process for at least the next 50 years, Grundy (2008), see Fig 1.1.

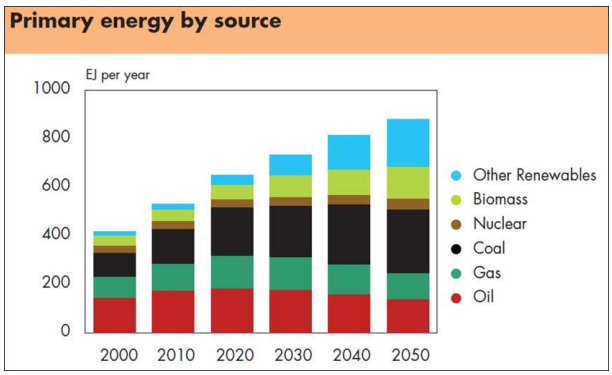

Figure 1.1: Shell energy consumption scenario for the next 50 years

During the past few years the development of combustor technology has followed a general trend towards fuel flexibility and increased use of bio fuels. Fuel flexibility is a term often used to describe the growing trend for gas turbines to be operated on a variable set of fuels. These fuels are typically of the type Low Caloric Value (LCV). The opportunity to operate on flexi-fuel is important since fossil fuels are a limited energy source. The use of syngas fuel (a mixture of CH_4, CO and H_2) in combustors is becoming more attractive since this is a common denominator for many gasification processes based on either bio fuels or fossil fuels.

Regulatory requirements for limiting the emissions of pollutants such as nitrogen oxides (NO_x), carbon monoxide (CO), unburned hydrocarbons (UHC) and carbon dioxide (CO_2) often limit the fuel supply and operability of lower cost fuels. For ideal stoichiometric combustion of hydrocarbon fuels, the reactants are fuel and oxidizer and the products are carbon dioxide CO_2 and water H_2O. But, for an incomplete combustion process emissions are produced such as soot, CO and UHC. The release of greenhouse gases, such as CO_2, is regarded as the main source of global warming. The most important factor that affects the NO_x production is the flame temperature. Lower temperature can be achieved by operating well away from the stoichiometric condition, but this results in increasing production of both CO and UHC, see Fig 1.2. Improved combustion technology in terms of efficiency and pollutant

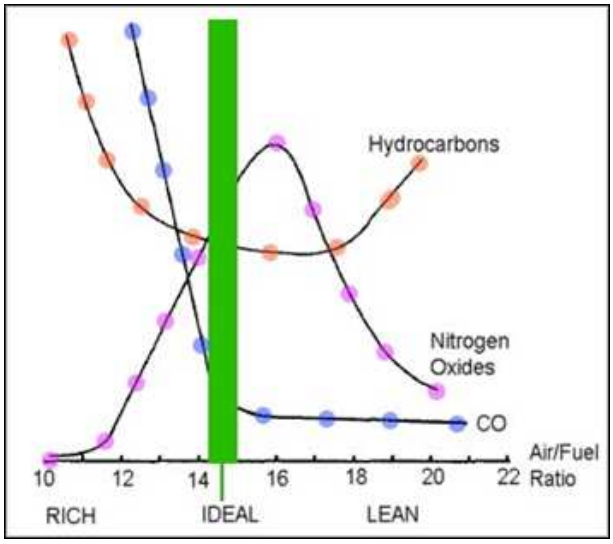

Figure 1.2: Effect of air/fuel ratio on gas emissions

emissions is therefore crucial since this reduces the NO_x production. Understanding the combustion behavior of flexi-fuels is very important since they have a significantly lower heating value than conventional fossil fuels.

This work involves derivation of new multi-step global mechanisms for methane-air mixture and syngas fuels, coupling these multi-step mechanisms with an established turbulence interaction model, CFD analysis for a premixed scaled 4^{th} generation Dry Low Emission (DLE) burner supplied by Siemens Industrial Turbomachinery (SIT) and comparison with experimental data from burner test rig at LTH/Combustion Physics. Also, a test case named Sandia Flame D has been modeled

with an optimized global reaction mechanism for methane-air mixture and compared to high quality experimental data.

1.2 Kinetic Modeling

Both the chemical kinetics and the interaction between turbulence and the chemical reactions involved have to be modeled accurately to predict the combustion process in the context of a detailed 3D CFD analysis. Increasing power and memory of computers and the possibility to run a simulation at several processors in parallel have made it possible to use more advanced turbulence models and more species and reactions included in the chemistry. But, the need for simplified chemistry and hence global reaction mechanisms is still important.

1.3 Turbulence-Chemistry Interaction

The addition of a large number of chemical species complicates the turbulent reaction modeling since the chemical reaction rates depend non-linearly on the species concentrations, Warnatz *et al.* (2006). Fast chemistry assumption is often made for turbulent reacting flow. This means that turbulent motions control the reaction rate, and hence simplifies the description of the reacting flow to that of a mixing problem. The eddy-breakup model (Spalding (1971), Spalding (1976) and the Eddy Dissipation Model (EDM), based on the work by Magnussen & Hjertager (1976) are examples of such models. The EDM is well known and used in the industry. In the EDM model the chemical reaction rate is governed by the turbulence mixing rate, ϵ/k.

More elaborate models also take into account finite-rate chemistry, for example the Eddy Dissipation Concept (EDC) by Gran & Magnussen (1996), PDF-methods (Pope (1985)), flamelet models (Peters (1986)) and the Partially Stirred Reactor model (Golovitchev *et al.* (2000)). The EDC model is an extension of the EDM model to include detailed chemical mechanisms in turbulent reacting flows. It assumes that reaction occurs in small turbulent structures, called the fine scales. These small scale structures can be captured as a part of the cell, where Kolmogorov-sized eddies containing combustion species are situated so close together that mixing on the molecular level is taking place. The EDC model evaluates the volume of each cell, where mixing on a molecular scale is occurring, and treats this part of the cell as a PSR.

1.4 Turbulence Modeling

Turbulent flows are characterized by a large range of length and time scales, see Fig 1.3. The turbulent spectrum is divided up into three different regions. The first region, I, corresponds to the generation of large energy containing scales. The intermediate region stands for the inertial subrange were the energy is transferred from large to small scales. In the third region, III, the small scales are dissipated. Depending on which turbulence model one use different amounts of the turbulent spectrum are resolved and modeled.

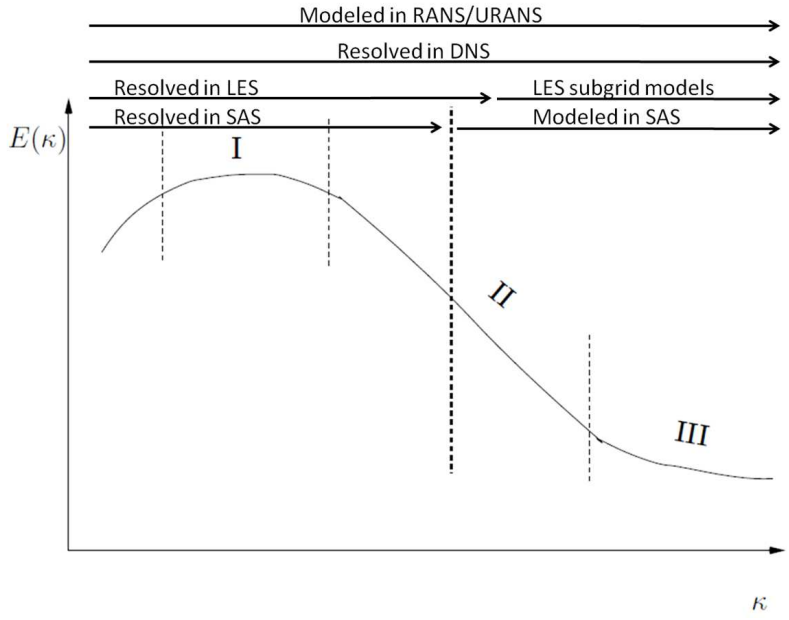

Figure 1.3: The turbulent spectrum

RANS models are very important turbulence models for engineers in everyday work. The models are robust and the turnaround time for the simulations is short. However, the RANS models give only the mean solution of a problem, which is not always that useful in the design of practical systems, since the mean solution does not really exist. In RANS the entire turbulent spectrum is modeled. The other extreme is to use Direct Numerical Simulation (DNS) where all the scales are resolved. However DNS is extremely expensive and will not be possible to use in the industry in the near future for the kind of applications that is considered here. LES resolves large-scale turbulent mixing and is the best candidate for simulating turbulent flames. The LES simulation gives good prediction of the flame front dynamics, which is of great help for NO_x predictions. Between the RANS models and the LES

model we have the hybrid RANS-LES models. These models switch to LES mode in unsteady flow if the resolution of the grid is satisfied and to an unsteady RANS mode close to the walls. Examples of the hybrid RANS-LES models are the Scale Adaptive Simulation (SAS) and the Detached Eddy Simulation (DES) models. The SAS approach represents a new class of the URANS models. Different from the RANS formulations, the SAS model adjusts the turbulence length scale to the local flow. As a measure of the local flow length scale, a boundary layer length scale introduced by von Karman is generalized for arbitrary three-dimensional flows. Both the SAS and the LES models are used for the transient simulations in the present work.

1.5 The Flexi-Fuel Burner

The premixed scaled 4^{th} generation Dry Low Emission (DLE) burner is supplied by Siemens Industrial Turbomachinery (SIT). The SIT burner consists of a complex arrangement of fuel and air premix ducts and swirler vanes, involving a main premixed flame (MAIN), a partially premixed pilot flame (PILOT) and a confined rich premixed lean flame (RPL), shown in Fig 4.3. The air and fuel are premixed before the com-

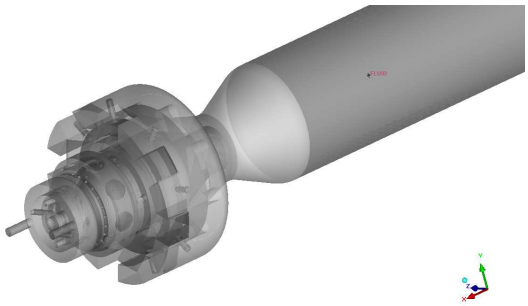

Figure 1.4: MAIN, PILOT and RPL systems

bustion process takes place. The RPL flame burns at rich conditions in a pre-combustion chamber, creating hot gases with high amounts of radicals. This hot gas is then mixed downstream of the RPL with premixed fuel/air from the MAIN and PILOT systems, which augments the overall flame in the tube.

1.6 Experimental Setup

The experiments were conducted at LTH in an atmospheric version of the burner test rig, see Fig 1.5. Fuel to each of the three sectors is in-

Figure 1.5: The burner setup at LTH

dividually controlled by Alicat Scientific Mass Flow Controllers (MFC). The air flow to the RPL is also controlled by an Alicat MFC, allowing independent control of the RPL sector. Air to the PILOT and MAIN sectors is supplied by two Rieschle SAP 300 blowers, which are controlled by a variable frequency AC driver. Flow meters at the blower outlet monitor air flow to the PILOT and MAIN sectors of the burner, whose design distributes 21% of the air to the PILOT and 79% to the MAIN sector. Blower control, flow monitoring and MFC's are all coupled to an in-house LabView control program. The experimental results are reported by Sigfrid *et al.* (2011*a*) and Sigfrid *et al.* (2011*b*).

Chapter 2

Kinetics

DETAILED reaction mechanisms for conventional and bio fuels are huge and contain hundreds of species and thousands of reactions. Run-time and convergence requirements, coupled with CFD codes, imply that there is still a need for simplified reaction mechanisms, despite the increasing power and memory of computers. The computational cost is dependent on both the number of chemical species and number of reactions involved in the simulation. By systematically decreasing the number of reactions and species, for a limited range of conditions, it is possible to construct simplified global reaction mechanisms that approximate the real chemical reactions in terms of major species, temperature, heat release, etc.

2.1 Global Reaction Mechanisms

Research on the development of reliable global reaction mechanisms for combustion of hydrocarbons was done during the 80s by WestBrook & Dryer (1984) and Jones & Lindstedt (1988). Westbrook and Dryer derived 1- and 2-step global reaction mechanisms for hydrocarbons fuels and are well known and often used in the industry. In the single step mechanism the fuel and oxidizer (air) reacts to give CO_2 and H_2O. The weakness of the single step mechanism is that by assuming that the reaction products only are CO_2 and H_2O the total heat of reaction is overpredicted. To account for this, a two step model for hydrocarbons was suggested by Westbrook and Dryer, which can be seen below for methane-air gas:

$$\begin{aligned} CH_4 + \frac{3}{2}O_2 &\Rightarrow CO + 2H_2O \\ CO + \frac{1}{2}O_2 &\Rightarrow CO_2 \end{aligned} \tag{2.1}$$

Jones & Lindstedt (1988) developed a 4-step global reaction mechanism for several hydrocarbon fuels. For methane-air mixture the global multi-step reaction mechanism involves the following steps:

$$\begin{aligned} CH_4 + \frac{1}{2}O_2 &\Rightarrow CO + 2H_2 \\ CH_4 + H_2O &\Rightarrow CO + 3H_2 \\ H_2 + \frac{1}{2}O_2 &\leftrightarrow H_2O \\ CO + H_2O &\leftrightarrow CO_2 + H_2 \end{aligned} \tag{2.2}$$

The first two reactions are global reactions in one direction, whereas the last two are equilibrium reactions. A promising new approach to construct global reaction mechanism was reported by Meredith & Black (2006). They address the difficulties in constructing global mechanisms by invoking a more mathematical approach. In brief, they apply robust optimization techniques to obtain a global mechanism that gives the best possible match with detailed chemistry. They report very good results with 3-/5-step global reaction mechanisms for methane and JP8 combustion cases.

Franzelli *et al.* (2010) used a slightly different but also promising approach. They derived a 2-step global reaction mechanism for kerosene combustion. To predict better results at rich conditions, they introduced correction functions, dependent on the local equivalence ratio, for the fuel oxidation and the CO oxidation. Furthermore, they based the backward rate of reaction 2 on an equilibrium assumption.

Cuoci *et al.* (2009) optimized two global reaction mechanisms using the work from WestBrook & Dryer (1984), Jones & Lindstedt (1988) and Andersen *et al.* (2009) as a starting point. The evaluation of the multi-step global reaction mechanisms were based on the regression data from a detailed kinetic scheme in laminar diffusive counter-flow flames. These flames were assumed as a good representation of the real flame (Buzzi & Manenti (2009), Peters (1984)). The work by Cuoci *et al.* (2009) was tested on a syngas flame with promising results.

The most frequently used global mechanisms are often determined by applying optimization techniques or by tuning to obtain the expected results in CFD simulations. Several different reduced reaction mechanisms of methane-air mixture and syngas exist in the literature, for example Novosselov & Malte (2008), Gokulakrishnan *et al.* (2006), Marlow & Norton (1995) and Slavinskaya *et al.* (2008). Unfor-

tunately, global mechanisms are typically only valid over limited operating ranges and cannot account for all of the possible combustion phenomena (e.g. NO_x, UHC, auto-ignition, etc). Also, the drawback of most of the published global mechanisms is that they are not flexible enough to cope with a wide range of equivalence ratios as is considered here (from 0.5 up to 1.6), which is necessary in order to handle the complex flame arrangement in the present swirl-stabilized flexi-fuel burner.

2.2 The Perfectly Stirred Reactor Model

The PSR is an ideal constant pressure reactor, in which perfect mixing is assumed inside the control volume, due to high diffusion rates or forced turbulent mixing. This means that the rate of conversion of reactants to products is controlled by chemical reaction rates and not by mixing processes. In addition to the fast mixing, the modeling of PSR requires that the flow through the reactor must be characterized by a residence time, τ_{res}, which is defined accordingly to:

$$\tau_{res} = \frac{V\rho}{\dot{m}} \tag{2.3}$$

where V is the reactor volume, ρ is the density inside the reactor and $\dot{m}$ is the mass flow through the reactor. The PSR reactor is assumed to be operating at steady-state, so there is no time dependence included in the equations. Fig 2.1 illustrates the conceptual representation of a PSR reactor.

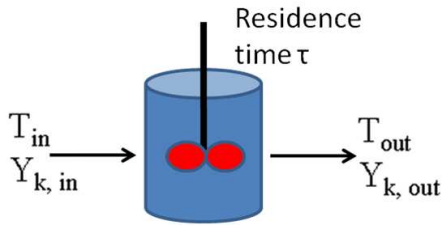

Figure 2.1: Schematic picture showing the PSR model

Reactants is introduced through the inlet with a given species composition and temperature. The reactor pressure is specified, so that the conservation equations determine the volume outflow. All properties are uniform inside the reactor (mass fractions, temperature and pressure). The gas leaving the reactor has the composition and temperature of the reactor $T_{out} = T$ and $Y_{i,out} = Y_i$. There is no heat loss,

which means that the reactor is adiabatic. The inlet conditions for the simulations for methane-air mixture are $P_{in} = 1atm$ with two different temperatures, $T_{in} = 295K$ and $T_{in} = 650K$. Different residence times and equivalence ratios are simulated and reported in paper I.

2.3 Optimization Strategy

The method chosen here is based on the idea that the global mechanism may first be locally optimized for a set of different equivalence ratios, and the Arrhenius rate coefficients involved for an arbitrary equivalence ratio can then be interpolated from these optimized values. The optimization at each equivalence ratio can be done in many different ways, but here we compare results of PSR calculations for both a detailed reference mechanism and the global reaction mechanism. A similar method was used by Meredith & Black (2006). An alternative optimization method is instead to match the laminar flame speed, this is used by Franzelli *et al.* (2010).

2.3.1 Methane-Air Mixture

Gri Mech 3.0 was chosen as the detailed reference reaction mechanism. This mechanism involves 325 reactions and is optimized to model natural gas combustion, Smith. *et al.* (1999). The goal of the first phase of the kinetic modeling work was to construct a multi-step global reaction mechanism for methane-air mixture that predicts temperatures and emissions over a wide range of combustion conditions, e.g. equivalence ratios 0.5 - 1.6, inlet temperatures 250K - 650K and atmospheric pressure. Meredith & Black (2006) 3-step reaction mechanism was used as a starting point for the optimization. The optimization of the 3-step global reaction mechanism was done in the following way.

- First, modifications of the Arrhenius rate coefficients (reaction orders, activation energy and pre-exponential factors) on a 3-step reaction mechanism were done to improve the predictions at rich conditions. Unfortunately, no improvements were achieved at rich conditions despite several attempts. The PSR code was used as a tool to judge whether the global reaction mechanism was performing well.

- The second phase was to modify the second (carbon monoxide oxidation) and third (carbon dioxide reduction) reactions to be a $CO - CO_2$ equilibrium reaction. This implied that the reaction orders were changed to comply with the standard reaction orders for an elementary

reaction. This modification improved the results slightly at rich conditions.

- The third phase was to use the PSR code to optimize the Arrhenius rate coefficients for the fuel oxidation into CO and H_2O and the $CO - CO_2$ equilibrium reaction at lean conditions. After this step the activation energies were held constant.

- The fourth phase was to optimize the pre-exponential factors at rich conditions.

- The fifth and last phase was to fit these optimized pre-exponential factors into correction functions. Here, the Franzelli *et al.* (2010) correction functions were used since their results were quite close to the optimized results that were obtained here. The correction functions were shifted slightly in terms of equivalence ratio.

To sum up, the optimization was performed in many steps, using the work of Meredith & Black (2006) and Franzelli *et al.* (2010) as a starting point. The improved global reaction mechanism is a result of the PSR optimization.

2.3.2 Syngas Mixture

Different syngas mixtures are experimentally investigated by Sigfrid *et al.* (2011*a*). The syngas mixtures consists of different amounts of methane, carbone monoxide and hydrogen. The latter species makes the optimization much more difficult since hydrogen burns relatively easy and has a low molecular weight. The current multi-step global reaction mechanism that is to be optimized in this project consists of 6-step global reactions and can be seen below:

$$\begin{aligned} CH_4 + \frac{1}{2}O_2 &\Rightarrow CO + 2H_2 \\ CH_4 + H_2O &\Rightarrow CO + 3H_2 \\ CO + \frac{1}{2}O_2 &\Leftrightarrow CO_2 \\ CO + H_2O &\Leftrightarrow CO_2 + H_2 \\ H_2 + \frac{1}{2}O_2 &\Rightarrow H_2O \\ H_2O &\Rightarrow H_2 + \frac{1}{2}O_2 \end{aligned} \tag{2.4}$$

2.4 Results of the Kinetic Optimization

The present optimized 3-step global reaction mechanism for methane-air gas mixture consists of two reactions:

$$\begin{aligned} 2CH_4 + 3O_2 &\Rightarrow 2CO + 4H_2O \\ 2CO + O_2 &\Leftrightarrow 2CO_2 \end{aligned} \tag{2.5}$$

where the first reaction is the oxidation of methane into CO and H_2O and the second reaction is the oxidation of CO into CO_2. The backward rate for the second reaction is based on an equilibrium assumption. Table 2.1 shows the optimized Arrhenius coefficients (activation energy, pre-exponential factor and temperature coefficient) that are used in the optimized 3-step global reaction mechanism.

Table 2.1: Activation energy E_a, pre-exponential factor A and temperature exponent β

Reaction	A	$E_a(J/kmol)$	β
$2CH_4 + 3O_2 \Rightarrow 2CO + 4H_2O$	1.398762e10	1.16712e8	-0.062
$2CO + O_2 \Leftrightarrow 2CO_2$	7.381123e11	7.65969e7	0.215

The reaction rates for the forward reactions are the following:

$$RR_1 = f_1(\phi) A_1 T^{\beta_1} e^{\frac{-Ea_1}{RT}} [CH_4]^{0.5} [O_2]^{1.066} \tag{2.6}$$

$$RR_2 = f_2(\phi) A_2 T^{\beta_2} e^{\frac{-Ea_2}{RT}} [CO_2]^2 [O_2]^1 \tag{2.7}$$

where A is the pre-exponential factor, E_a is the activation energy, R is the gas constant, T is the temperature and f_1 and f_2 are the correction functions accordingly to Fig 2.2. The reaction orders for the first reaction are the same as Meredith & Black (2006) used. No correction is needed for lean conditions, $\phi < 1$, since the optimized 3-step global reaction mechanism predicts temperatures and emissions sufficiently well in this region. This implies that both correction functions remain constant, equal to one, and have no impact on the reaction rates. The production of CO_2 is reduced for rich mixtures when the equivalence ratio increases. This is done using correction function f_1, which increases the rate of oxidation of methane. At the same time, the reaction rate in the second reaction in the optimized 3-step global reaction scheme needs to be reduced. Thus function f_2 corrects the description of the equilibrium state. For rich combustion, correction function f_2 decreases with the equivalence ratio in order to decrease pre-exponential factor A_2 and to reduce the oxidation of CO to CO_2. The 3-step global reaction

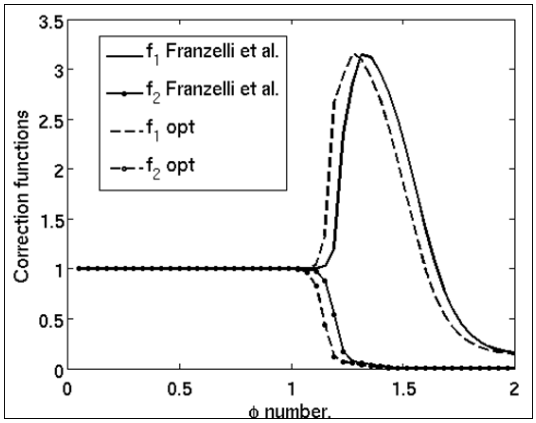

Figure 2.2: Plot showing the correction functions f_1 and f_2

mechanism is optimized against a detailed reference mechanism, GRI Mech 3.0, Smith. *et al.* (1999), for PSR calculations. The CANTERA software has been used for the detailed mechanism simulations and an in-house PSR code for the global reaction mechanism. Fig 2.3 shows comparison between the optimized 3-step global reaction mechanism and the reference detailed reaction mechanism. The results show that the reactor temperature is reasonably well predicted for both lean and rich conditions for T_{in}=295K and atmospheric pressure. More results from the kinetic optimization can be found in paper I.

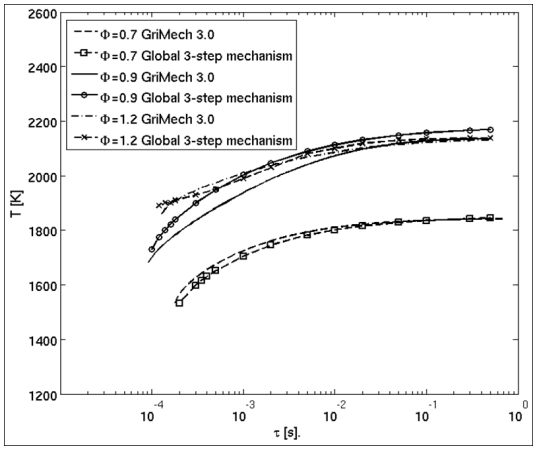

Figure 2.3: Plot showing temperature comparisons of a detailed mechanism (Gri Mech 3.0) and optimized 3-step global mechanism for methane-air gas mixture at equivalence ratios of 0.7, 0.9 and 1.2, T_{in}=295K and atmospheric pressure

2.5 Flame Speed

The laminar flame speed is the velocity at which the flame front propagates relative to the flow of the unburnt mixture. The laminar flame speed depends on the pressure, the fresh-air temperature and the equivalence ratio. In Fig 2.4 the laminar flame speed is calculated for three different global reaction mechanisms and for the detailed mechanism. The present optimized global reaction mechanism capture the laminar flames speed reasonably well at $\phi < 1.2$ and $\phi > 1.6$, but overpredicted in the range of $1.2 < \phi < 1.6$ due to the correction functions. The opti-

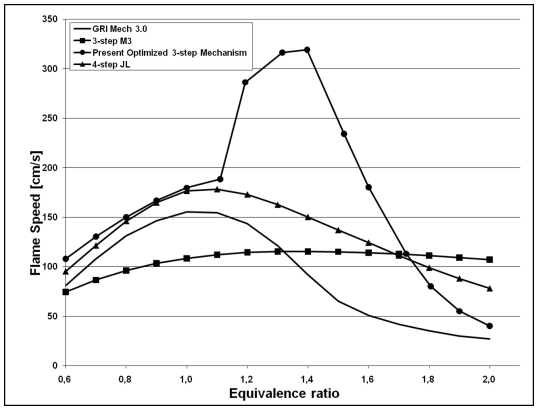

Figure 2.4: Laminar flame speed: Detailed mechanism GRI Mech 3.0, 3-step global mechanism by Meredith & Black (2006), present optimized 3-step global mechanism and 4-step global mechanism by Jones & Lindstedt (1988) T_{in}**=650K**

mization work presented in this thesis was based on temperature and emissions matching between the detailed mechanism and the global reaction mechanism using the PSR model. An alternative way is instead to select an optimization method which match the laminar flame speed. The conclusion from the kinetic optimization is that it seems impossible to match both PSR results and laminar flame speed. The question is if the optimization based on the laminar flame speed would give different correction functions and how much different from those from the PSR optimization? This is not known at present and will be looked into in future work.

Chapter 3

Combustion and CFD

3.1 Turbulent Combustion

A combined turbulence-chemistry interaction model, the Finite Rate Chemistry/Eddy Dissipation Model (FRC/EDM), in Ansys CFX, was chosen for all CFD analyses. The combined FRC/EDM model gives two different reaction rates for each reaction, one from the EDM model and one from the FRC model. The minimum rate for each reaction is then chosen in the CFD-simulations.

3.2 FRC Model

The FRC model computes the reaction rate from the following expression:

$$R_k = (F_k \prod_{I=A,B..}^{N_c} [I]^{\nu_{kl}^{'}} - B_k \prod_{I=A,B..}^{N_c} [I]^{\nu_{kl}^{''}}) \tag{3.1}$$

where $[I]$ is the molar concentration of component I and F_k and B_k are the forward and the backward rate constants respectively. $\nu_{kI}^{'}$ and $\nu_{kI}^{''}$ represent the reaction order of component I in the reaction k. This reaction order is equal to the stoichiometric coefficient for elementary reactions, but it can be different for global reactions. The forward and backward rate constants assume Arrhenius temperature dependence according to:

$$F_k = A_k T^{\beta_k} e^{\frac{-E_k}{RT}} \tag{3.2}$$

$$B_k = \frac{F_k}{K_c} \tag{3.3}$$

where A_k is the pre-exponential factor, β_k is the temperature exponent, E_k is the activation energy and K_c the equilibrium constant. The FRC model computes one reaction rate respectively for each reaction in the optimized global reaction mechanism.

3.3 EDM Model

In the EDM model, the reaction rate of reaction k is computed as:

$$R_k = A\frac{\varepsilon}{k} min\left(\frac{[I]}{\nu_{kI}^{'}}\right) \tag{3.4}$$

where A is a constant, $\frac{\varepsilon}{k}$ is the turbulent mixing rate, $[I]$ is the molar concentration of component I and $\nu_{kI}^{'}$ represent the reaction order of component I in the elementary reaction k. The EDM model computes one reaction rate respectively for each reaction in the optimized global reaction mechanism. The EDM model is based on the work of by Magnussen & Hjertager (1976).

Chapter 4

Geometry and Mesh

4.1 The SGT 750 Engine

The SGT 750 is the latest gas turbine development from Siemens Industrial Turbomachinery AB, Fig 4.1, which is characterized by high efficiency and reliability. Aiming for higher efficiency in the design of gas turbines implies higher combustion temperatures and higher pressure ratios. The SGT 750 has eight combustor cans, the 4^{th} generation DLE burners. The gas turbine can be run on a set of different fuels with on-load switchover between the fuels.

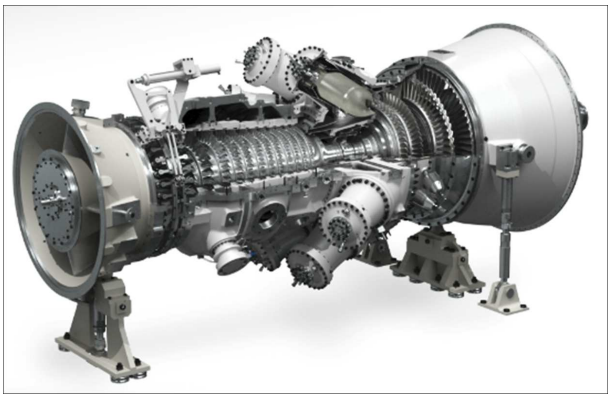

Figure 4.1: A Cut Through the SGT 750 Engine

Each burner consists of three different systems, the MAIN, the PILOT and the RPL part. Fig 4.2 shows the burner in the SGT 750 engine.

Figure 4.2: 4^{th} generation DLE burner

4.2 CFD-Model of the Scaled Flexi-Fuel Burner

The premixed scaled 4^{th} generation DLE burner is supplied by SIT and was developed to be fuel flexible. The real SIT burner geometry differs from the prototype used in the test rig at LTH. The main differences are the air path into the main system and the scaling of the burner. The real SIT burner has a radial inlet for the main air system while the prototype has an axial one. The prototype has also a scaled RPL part. The CFD-model has the same geometry as the LTH test rig. The high swirl flow in the SIT burner is extremely challenging from an aerodynamic and combustion point of view, especially since the combustor consists of comprised of a lean premixed MAIN part, a partially premixed PILOT and an RPL radical pool generator. These systems together create a complex geometry with many details included, see Fig 4.3. The burner is composed of three concentric sectors each with its own equivalence ratio control. The burner can be coupled to either a square or a cylindrical combustion liner, which terminates in a conical contraction before dumping to exhaust.

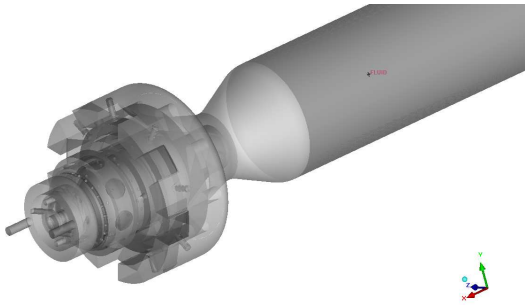

Figure 4.3: CFD-Model with a cylindrical liner

4.3 Hexahedral Meshing

The grid generation of the scaled 4^{th} generation DLE flexi-fuel burner required a lot of effort since only structured hexahedral (hex)-cells were used and all the cavities, inlets, ribs, swirler vanes etc were included in the CFD-domain, see Fig 4.4 - Fig 4.9. The hex mesh is preferred over tetrahedral mesh since the hex-cells give lower numerical dissipation (the mesh cells are aligned with the general flow direction) and lower cell count (a factor of 8 lower). It is extremely important to keep the cell count down since it is direct proportional to the simulation time needed for a converged solution. A grid independence study was done both for the steady-state run and transient run. To decide if the grid is mesh independent, transient averaged data as temperatures and major species (CH_4, CO_2 and CO) were compared for different hexahedral grids at different planes downstream in the burner. The number of cells finally used was between 9-17 Mcells depending on which turbulence model that was used.

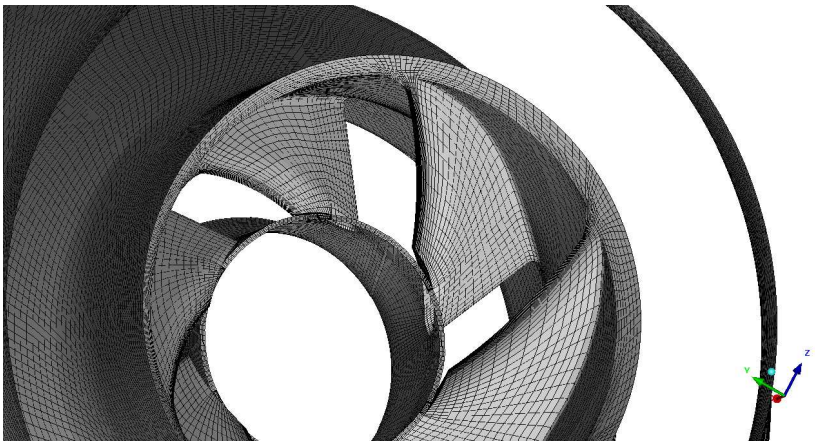

Figure 4.4: Swirler vanes for the RPL system

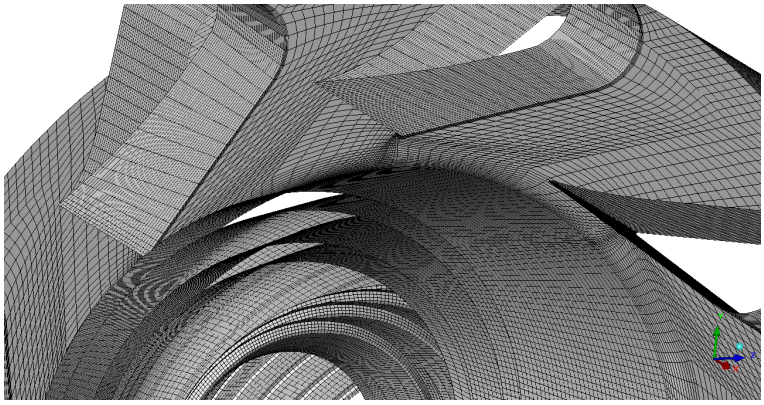

Figure 4.5: Swirler vanes for the MAIN system and ribs

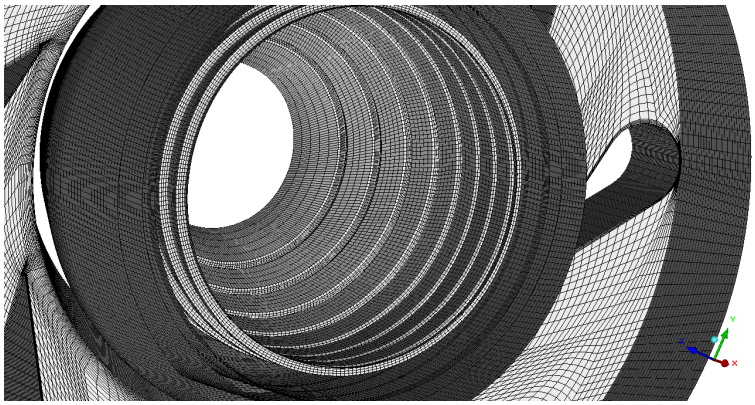

Figure 4.6: Swirler vanes for the MAIN system and ribs

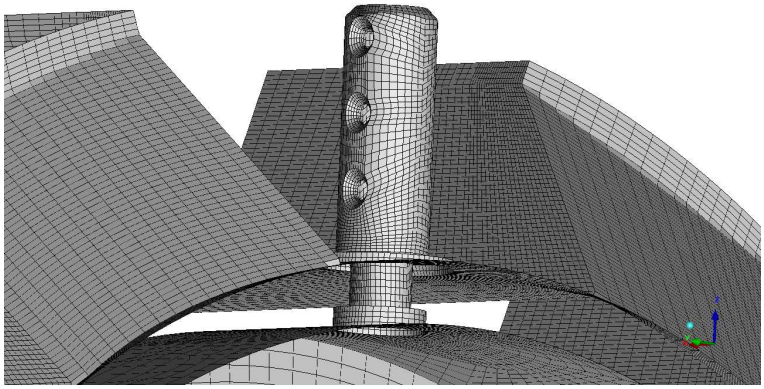

Figure 4.7: Fuel injectors for the MAIN system - Rods

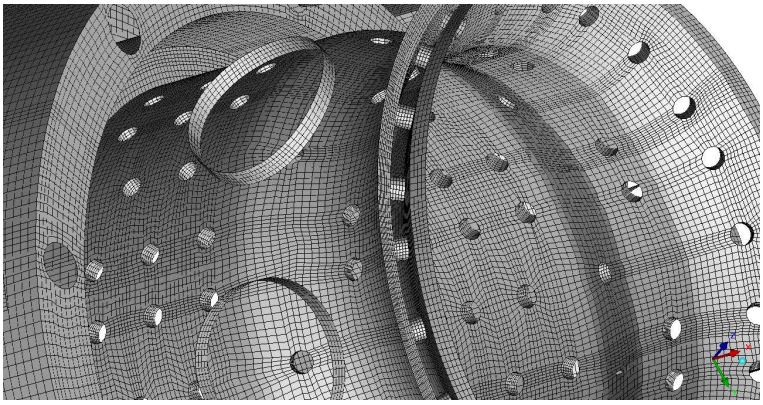

Figure 4.8: Cooling holes and cavities

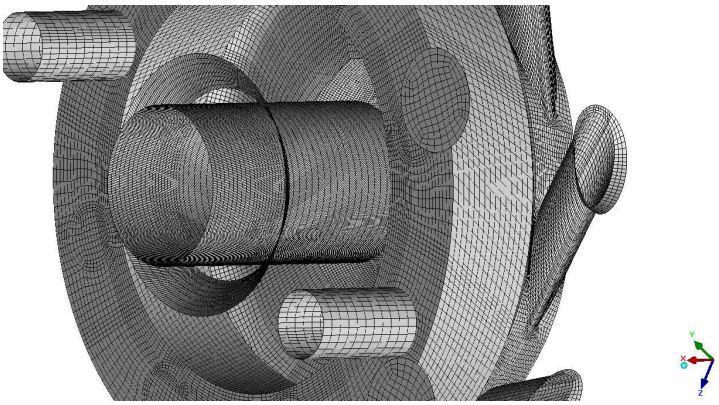

Figure 4.9: Inlets and cavities upstream in the burner

Chapter 5

Numerical Method and Turbulence Modeling

5.1 Introduction

The Ansys CFX commercial software package was used to solve for steady-state and transient simulations. Both the $k-\omega$ SST turbulence model by Menter (1994) and the Re-Normalisation Group (RNG) $k-\epsilon$ turbulence model by Yakhot *et al.* (1992) were selected for the steady-state simulations. A NOx model was also included for the steady-state simulations. The model calculates NO produced in the combustion process and does not affect the main combustion calculation since the NO concentrations are typically very low. In Ansys CFX, the NO model is implemented by the Zeldovich mechanism using the Arrhenius temperature probability density function option. The SAS-SST by Egorov & Menter (2007) and LES-Wall Adapting Local Eddy Viscosity (WALE) by Nicoud & Ducros (1999) turbulence models were used for the transient simulations.

5.2 Governing Equations

The transport equations that describe the unsteady flow for reacting flow are conservation of mass, species, momentum and energy. The equations follow here:

Conservation of mass:

$$\frac{\partial \rho}{\partial t} + \frac{\partial}{\partial x_j}\left(\rho u_j\right) = 0 \tag{5.1}$$

Conservation of species:

$$\frac{\partial \rho Y_k}{\partial t} + \frac{\partial}{\partial x_i}\left[\rho(u_i + U_{k,i})Y_k\right] = \dot{w}_k \tag{5.2}$$

Conservation of momentum:

$$\begin{aligned}\rho\left[\frac{\partial u_i}{\partial t} + u_j\frac{\partial u_i}{\partial x_j}\right] = \frac{\partial}{\partial x_j}\Bigg[-p\delta_{ij} + \left(\mu_t - \frac{2}{3}\mu\right)\frac{\partial u_k}{\partial x_k}\delta_{ij} \\ +\mu\left(\frac{\partial u_i}{\partial x_j} + \frac{\partial u_j}{\partial x_i}\right) + \rho\left(\sum_{k=1}^{N} Y_k f_k\right)_i\end{aligned} \tag{5.3}$$

Conservation of energy:

$$\begin{aligned}\frac{\partial \rho h_0}{\partial t} + \frac{\partial}{\partial x_i}\left(\rho u_i h_0\right) - \frac{\partial p}{\partial t} = \dot{Q} - \frac{\partial q_i}{\partial x_i} + \\ \frac{\partial\left(u_i \tau_{ji}\right)}{\partial x_j} + \rho\sum_{k=1}^{N} Y_k f_{k,i}\cdot(u_i + U_{k,i})\end{aligned} \tag{5.4}$$

5.3 $k-\omega$ SST

The $k-\omega$ SST model is an industry standard for complex flows with separation and has become very popular. The $k-\omega$ SST model combines two different approaches. The model can be used all the way down to the wall without any extra damping functions. In the outer region (free-stream) the SST formulation switches to a $k-\epsilon$ behaviour. The k-equation reads:

$$\frac{\partial \rho k}{\partial t} + \frac{\partial}{\partial x_j}\left(\rho\bar{U}_j k\right) = \frac{\partial}{\partial x_j}\left[\left(\mu + \frac{\mu_t}{\sigma_k}\right)\frac{\partial k}{\partial x_j}\right] + P_k - \rho\beta^* k\omega \tag{5.5}$$

and the ω equation reads:

$$\begin{aligned}\frac{\partial \rho\omega}{\partial t} + \frac{\partial}{\partial x_j}\left(\rho\bar{U}_j\omega\right) = \frac{\partial}{\partial x_j}\left[\left(\mu + \frac{\mu_t}{\sigma_\omega}\right)\frac{\partial \omega}{\partial x_j}\right] + \alpha\frac{\omega}{k}P_k - \rho\beta\omega^2 \\ + (1-F_1)\frac{2\rho}{\sigma_{\omega 2}}\frac{1}{\omega}\frac{\partial k}{\partial x_i}\frac{\partial \omega}{\partial x_i}\end{aligned} \tag{5.6}$$

5.4 RNG $k-\epsilon$

The RNG model was developed by Yakhot *et al.* (1992) to renormalise the Navier-Stokes equations. The RNG approach is based on that the

equation attempts to account for the different scales of motion in the flow through modifications of the production term, P_k. The k-equation reads:

$$\frac{\partial \rho k}{\partial t} + \frac{\partial}{\partial x_j}\left(\rho \bar{U}_j k\right) = \frac{\partial}{\partial x_j}\left[\left(\mu + \frac{\mu_t}{\sigma_k}\right)\frac{\partial k}{\partial x_j}\right] + P_k - \rho\epsilon \tag{5.7}$$

and the ϵ equation reads:

$$\frac{\partial \rho \epsilon}{\partial t} + \frac{\partial}{\partial x_j}\left(\rho \bar{U}_j \epsilon\right) = \frac{\partial}{\partial x_j}\left[\left(\mu + \frac{\mu_t}{\sigma_\epsilon}\right)\frac{\partial \epsilon}{\partial x_j}\right] + C_{1\epsilon}\frac{\epsilon}{k}P_k - \rho C^{\star}_{2\epsilon}\frac{\epsilon^2}{k} \tag{5.8}$$

5.5 SAS-SST

The SAS approach represents a new class of the URANS models. The von Karman length scale explicitly enters the transport equations to the SAS model. The model gives suitable RANS solutions for stable flows. For flows with transient behavior the model reduces its eddy viscosity according to the locally resolved vortex size represented by the von Karman length scale. The SAS model can under those conditions allow the break-up of large unsteady structures into a turbulent spectrum and avoids RANS-typical single-mode vortex structure. SAS modeling is based on the use of a second mechanical scale in the source/sink terms of the underlying turbulence model.

The modified ω equation reads:

$$\begin{aligned}\frac{\partial \rho \omega}{\partial t} + \frac{\partial}{\partial x_j}\left(\rho \bar{U}_j \omega\right) = \frac{\partial}{\partial x_j}\left[\left(\mu + \frac{\mu_t}{\sigma_\omega}\right)\frac{\partial \omega}{\partial x_j}\right] + \alpha\frac{\omega}{k}P_k - \rho\beta\omega^2 \\ + (1 - F_1)\frac{2\rho}{\sigma_{\omega 2}}\frac{1}{\omega}\frac{\partial k}{\partial x_i}\frac{\partial \omega}{\partial x_i} + S_{SAS}\end{aligned} \tag{5.9}$$

The term S_{SAS} stands for the SAS source term and comes from a term in Rotta's transport equation for the correlation-based length scale, see Menter (1994).

The source term reads:

$$S_{SAS} = max\left[\zeta_2 \kappa S^2 \left(\frac{L}{L_{\nu k}}\right)^2 - C\frac{2\rho k}{\sigma_\phi} max\left(\frac{1}{\omega^2}\frac{\partial \omega}{\partial x_j}\frac{\partial \omega}{\partial x_j}, \frac{1}{k^2}\frac{\partial k}{\partial x_j}\frac{\partial k}{\partial x_j}\right), 0\right] \tag{5.10}$$

and the $L_{\nu k}$, L and constants read:

$$L_{\nu k} = \frac{\kappa \frac{\partial \bar{U}}{\partial y}}{\frac{\partial^2 \bar{U}}{\partial y^2}}$$

$$L = \frac{k^{1/2}}{\omega C_{\mu}^{1/4}}$$

$$C = 2$$

$$\zeta = 3.51$$

Chapter 6

CFD Results

THE main important CFD-results are compared to measurements data from LTH and reported in paper I and II. Some of the important results are presented and highlighted in this chapter.

6.1 Boundary Conditions

The mass flow rates for the different systems were obtained from measurements at LTH. Mass flow rates are set on the different inlets in the CFD-domain and are visible in Fig 6.1.

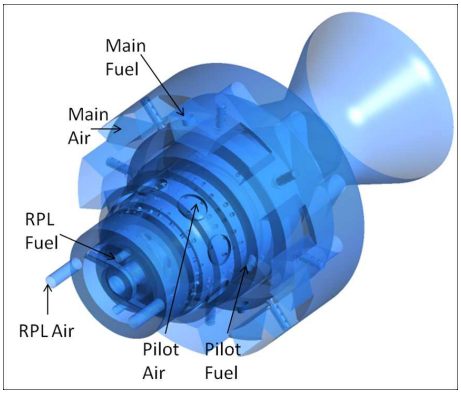

Figure 6.1: The burner inlets for fuel and air

The preheat temperature 650K was set for the air inlets and 300K at the fuel inlets. The outlet pressure boundary condition was set to a pressure outlet at atmospheric pressure. All the walls in the CFD-domain were set to adiabatic walls.

6.2 Swirl Number

The swirl number is defined accordingly to:

$$S = \frac{\int_{r_i}^{r_o} \rho\, u\, wr^2\, dr}{r_o \int_{r_i}^{r_o} \rho\, u^2 r\, dr} \tag{6.1}$$

where ρ is the density, u is the axial velocity, w is the tangential velocity, r_i is the inner diameter and r_o is the outer diameter. Fig 6.2 shows the local swirl number at the throat, which is located close to the RPL exit. The inner channel in the plot represents the RPL and PILOT systems together, while the outer channel represents the MAIN system. The average swirl number for the burner is approximately 0.8. The swirl number in the outer channel is above one and is therefore sufficiently high to break down the vortex structure and create a strong recirculation zone.

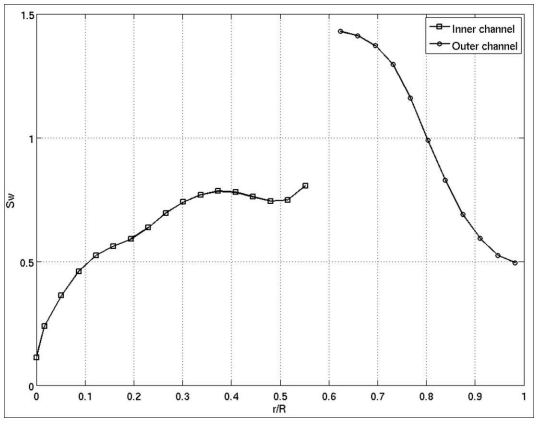

Figure 6.2: The local swirl number plotted in radial direction, $r = 0$ is the center of the burner

6.3 SAS-SST Results

The Ansys CFX commercial software package was used as CFD-solver. The computational mesh contained approximately 10 Mcells for the SAS-SST model. The CFL number was around 7-8 in average. The timestep for the simulation was 1e-5s.

6.3.1 Flow Field

Fig 6.3 shows the recirculation zone and a contour plot of the time-averaged axial velocity at a cross-sectional plane. The highest velocity

is located in the throat section. Fig 6.4 shows streamlines released from the inlets to the three different systems. The combustion products from the RPL, the fresh air and the fuel from the MAIN and PILOT systems are integrated and mixed in the quarl section before the second flame is obtained.

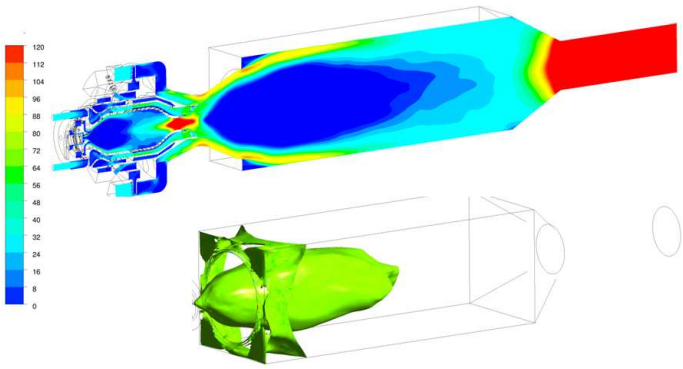

Figure 6.3: The upper plot shows the time averaged axial velocity and the lower one shows the recirculation zone

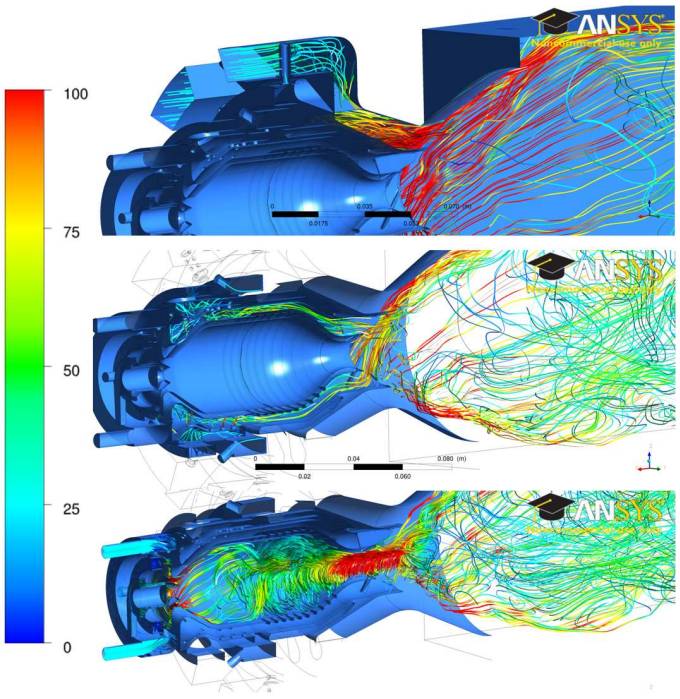

Figure 6.4: Streamlines released from the inlets to the three different systems. Upper one MAIN, middle one PILOT and lower one RPL

6.3.2 Temperature

Fig 6.5 shows contour plot of the time-averaged temperatures and the equivalence ratio in the burner. The highest temperature is located close to throat exit, were the stoichiometric condition is obtained. The figure also shows that the total equivalence is approximately 0.5 in the burner and the flow field is well mixed downstream with a uniform temperature distribution. This is important since the turbine life cycle decreases with non-uniform temperature distribution.

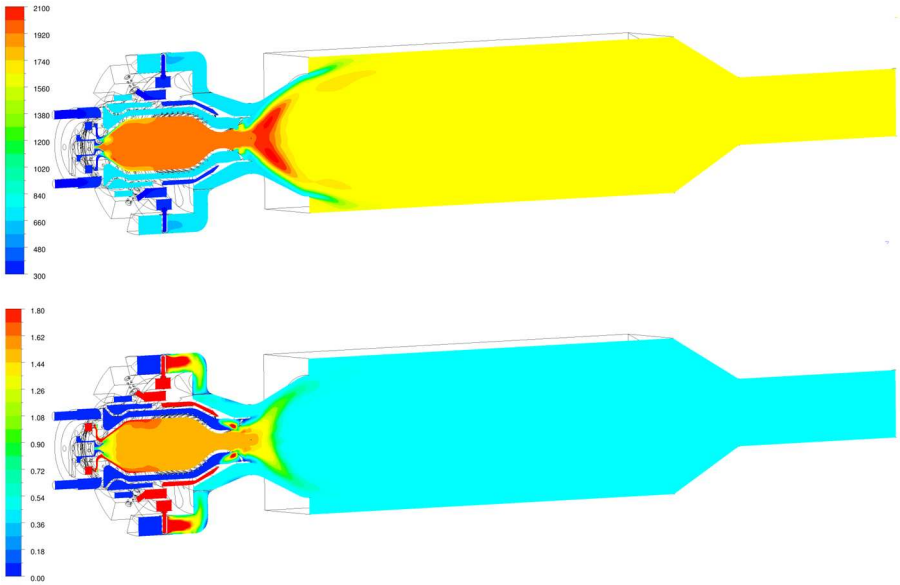

Figure 6.5: Upper plot: Time-averaged temperatures, lower plot: equivalence ratio in the burner

6.4 LES-WALE Results

The Ansys CFX software was also used to solve the LES simulation. The LES WALE model was used. This model is based on an algebraic 0-equation model and retains the simplicity of Smagorinskys model. The wall damping effects are accounted for without using the damping function explicitly. The computational mesh contained approximately 17 M hexahedral cells. The average CFL number was around 0.6 and the timestep was set to 1e-6s. Fig 6.6 shows regions with the highest swirling strength in the CFD-domain. These regions are located in the quarl and upstream position in the liner.
Fig 6.7 shows a contour plot of the time-averaged temperature at a

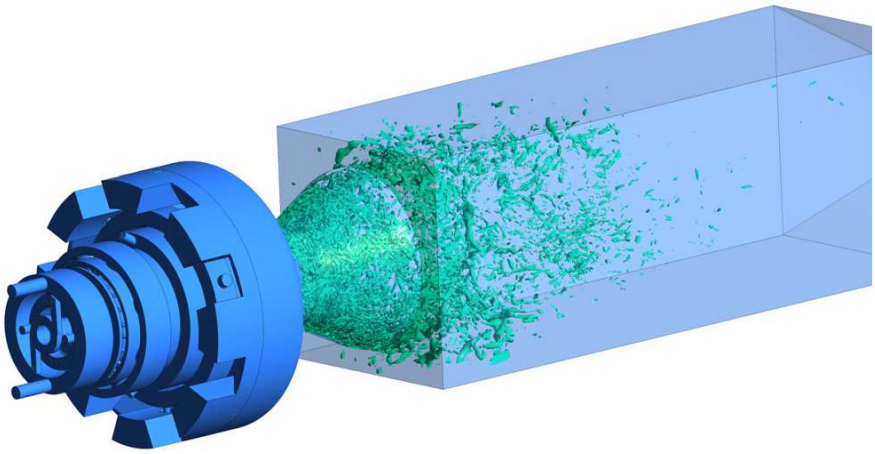

Figure 6.6: Iso-regions with the highest swirling strength in the CFD-domain

cross-sectional plane. The highest temperature is located in the quarl were the equivalence ratio is one.

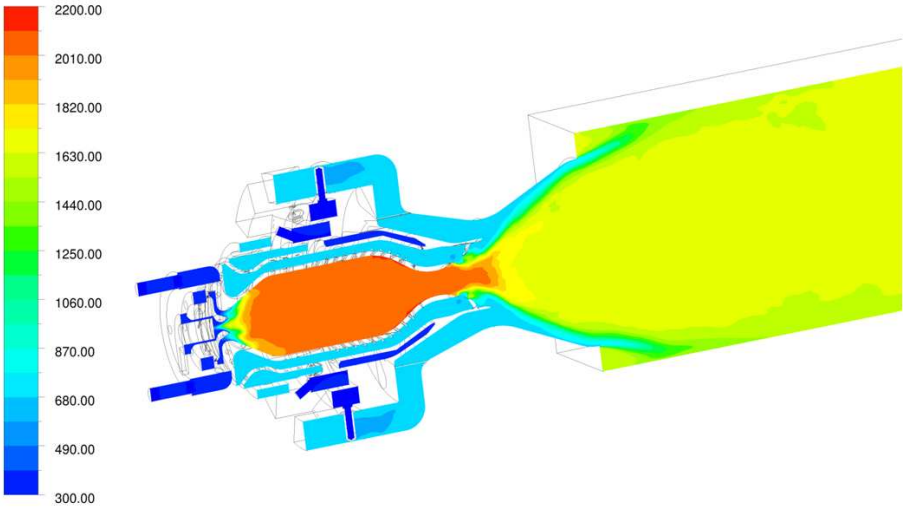

Figure 6.7: The time-averaged temperatures

Fig 6.8 shows the contour plot of the CO concentration, the lower a snapshot in time and the upper one the time-averaged values. The snapshot in time shows that small eddies with typical pattern is obtained in the reaction zone located in the quarl.

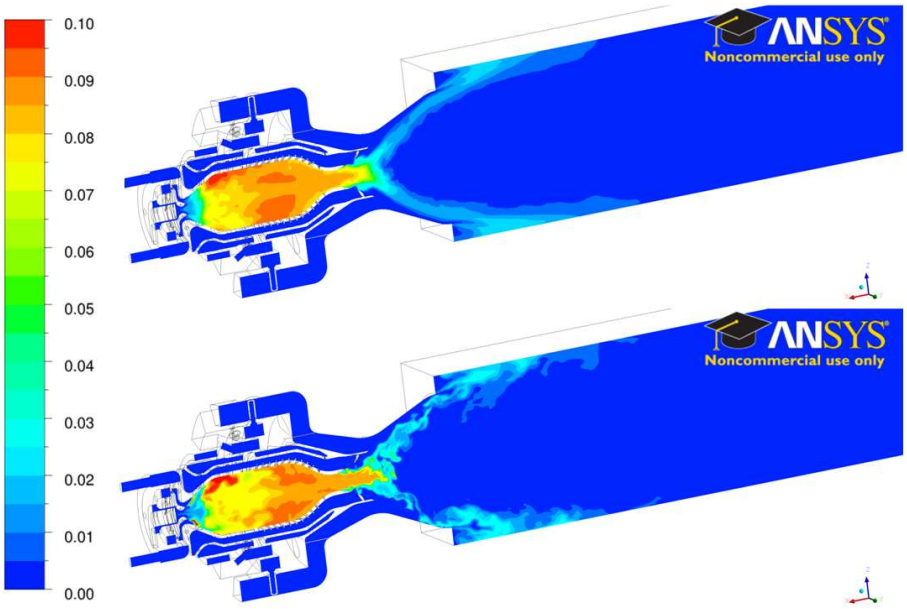

Figure 6.8: The upper plot shows the time-averaged CO concentration and the lower one shows the instantaneously CO concentration plot

Chapter 7

Summary of Papers

THIS chapter gives a short summary of the work done and the results reported in the three papers on which this thesis is based.

7.1 Paper I

7.1.1 Motivation and Work

Paper 1 presents the results of the kinetic optimization (3-step global reaction mechanism for methane-air mixture). The mechanism is derived, evaluated and applied in CFD analyses. The paper also presents numerical results of the 4^{th} generation SIT flexi-fuel burner using this optimized 3-step global reaction mechanism. The numerical results are compared with emission data.

7.1.2 Results

The reaction rates in the 3-step global reaction mechanism are optimized against a detailed reference mechanism (Gri Mech 3.0) for PSR calculations. The range of validity of the present global mechanism is equivalence ratios 0.5-1.6, atmospheric pressure and inlet temperatures corresponding to 295K-650K. The CFD results show reasonably good agreement with flame visualization and gas composition. The results of the 3-step global reaction mechanism show good agreement with experimental data for the CO value. The predicted flame position and shape are also close to the design intentions.

7.2 Paper II

7.2.1 Motivation and Work

Paper 2 presents numerical results from the 4^{th} generation SIT flexi-fuel burner, with three different configurations, which has been modeled with the optimized 3-step global reaction mechanism using CFD. The numerical results are compared with emission data at several points, velocity profiles at different locations and OH-PLIF images.

7.2.2 Results

The results from the circular liner show that the emission data (CO and O_2) are well predicted with the CFD simulations. The results from the second case with the squared liner show that the velocity field and the flame position are well predicted with the SAS-SST model, while the steady-state RANS fails in some regions. The velocity field in the open liner (unconfined flame) is not well captured by the CFD simulations.

7.3 Paper III

7.3.1 Motivation and Work

Paper 3 presents numerical results of the Sandia Flame D burner with the optimized 3-step reaction mechanism and WD2 using CFD. The numerical results are compared to emission, velocity and temperature profiles at different locations.

7.3.2 Results

The CFD results with the 3-step global reaction mechanism show reasonable agreement with the experimental data based on emission, velocity and temperature profiles, while the 2-step WD2 global reaction mechanism fails to predict the emission profiles in some regions.

Chapter 8

Concluding Remarks

An optimized 3-step global reaction mechanism for methane-air mixtures is derived, evaluated and applied in CFD analyses. The reaction rates in the 3-step global reaction mechanism are optimized against a detailed reference mechanism (Gri Mech 3.0) for PSR calculations. The range of validity of the present global mechanism is equivalence ratios 0.5-1.6, atmospheric pressure and inlet temperatures corresponding to 295K-650K.

The flow and temperature fields in the atmospheric test rig at LTH have been simulated with RANS, hybrid URANS/LES and LES solvers using the full geometry of the burner. The results are compared to the available experimental data (velocity profiles, emission data and OH-PLIF measurements).

The Sandia Flame D has also been modeled with the optimized 3-step scheme and WD2 using CFD. The results are compared to the available experimental data (emissions, velocity and temperature profiles).

Future Work

The intention for future work is to use the same optimization approach used for methane-air mixture to develop new optimized global reaction mechanisms for different low heating value gases, e.g. syngas. The ModeFrontier and CHEMKIN software packages are going to be integrated in the optimization loop. The target for the PSR optimization has been to match the temperatures at different equivalence ratios for the detailed and the global reaction mechanism. The intention for future work is to study how much the global reaction mechanism changes if the laminar flame speed is matched instead of the temperatures in a

PSR.

Only the FRC-EDM model has so far been used for the turbulence-chemistry interaction. More models on the finite rate chemistry part are going to be evaluated, e.g. the partially stirred reactor model.

The aim for future work is also going to be to compare the CFD simulations with more available data from LTH considering the LCV fuels.

Bibliography

ANDERSEN, J., RASMUSSEN, C. L., GISELSSON, T. & GLARBORG, P. 2009 *Energy Fuels* **23**, 1379–1389.

BUZZI, G. F. & MANENTI, F. 2009 *Chem. Eng. Science* **64**, 1061.

CUOCI, A., FRASSOLDATI, A., FARAVELLI, T. & RANZI, E. 2009 Accuracy and flexibility of simplified kinetic models for cfd applications. *32nd Meeting on Combustion* .

EGOROV, Y. & MENTER, F. 2007 Development and application of sst-sas turbulence model in the desider project. *Second Symposium on Hybrid RANS-LES Methods, Corfu, Greece* .

FRANZELLI, B., RIBER, E., SANJOSE, M. & POINSOT, T. 2010 A two-step chemical scheme for kerosene-air flames. *Combustion and Flame* **175**, 1364–1373.

GOKULAKRISHNAN, P., KWON, S., HAMER, A., KLASSEN, M. & ROBY, R. 2006 Reduced kinetic mechanism for reactive flow simulation of syngas/methane combustion at gas turbine conditions. *ASME Turbo Power Expo, Power for land , Sea and Air, GT2006-90573* .

GOLOVITCHEV, V. I., NORDIN, N., JARNICKI, R. & CHOMIAK, J. 2000 3-d diesel spray simulations using a new detailed chemistry turbulent combustion model. *International Spring Fuels Lubricants Meeting Exposition Paris, France June 19-22, 2000* .

GRAN, I. & MAGNUSSEN, B. F. 1996 *Combustion Science Technology* **119**, 171–217.

GRUNDY, P. 2008 Shell energy scenarios to 2050 .

JONES, W. & LINDSTEDT, R. 1988 Global reaction schemes for hydrocarbon combustion. *Combustion and Flame* **73**, 233–249.

MAGNUSSEN, B. F. & HJERTAGER, B. H. 1976 On mathematical models of turbulent combustion with special emphasis on soot formation and combustion. *16th Symp. (Int'l.) on Combustion* .

MARLOW, D. & NORTON, T. 1995 A reduced mechanism for low-heating-value gas combustion in a perfectly stirred reactor. *American Flame Research Committee International Symposium* .

MENTER, F. 1994 Two-equation eddy-viscosity turbulence models for engineering applications. *AIAA-Journal* **32**, 1598 – 1605.

MEREDITH, K. V. & BLACK, D. L. 2006 Automated global mechanisms generation for use in cfd simulations. *AIAA Journal* .

NICOUD, F. & DUCROS, F. 1999 Subgrid-scale modelling based on the square of the velocity gradient tensor. *Flow, Turbulence and Combustion* **62**, 183–200.

NOVOSSELOV, I. V. & MALTE, P. C. 2008 Development and application of an eight-step global mechanism for cfd and crn simulation of lean-premixed combustors. *Journal of Engineering for Gas Turbines and Power* **130**.

PETERS, N. 1984 Laminar flamelet concepts in turbulent combustion. *Prog. Energy Combust. Sci.* **10**, 319.

PETERS, N. 1986 Laminar flamelet concepts in turbulent combustion. *Proc. Combust. Inst.* **21**, 1231–1250.

POPE, S. B. 1985 Pdf methods for turbulent reactive flows. *Prog. Energy Combust. Sci.* **11**, 119–192.

SIGFRID, I., WHIDDON, R., COLLIN, R. & KLINGMANN, J. 2011*a* Experimental investigation of lean stability limit of an prototype syngas burner for low calorific value gases. *ASME Turbo Power Expo, Power for land , Sea and Air, GT2011-45694* .

SIGFRID, I., WHIDDON, R., COLLIN, R. & KLINGMANN, J. 2011*b* Parametric study of emissions from low calorific value syngas combustion, with variation of fuel distribution, in a prototype three sector burner. *ASME Turbo Power Expo, Power for land , Sea and Air, GT2011-45689* .

SLAVINSKAYA, N., BRAUN-UNKHOFF, M. & P.FRANK 2008 Reduced reaction mechanisms for methane and syngas combustion in gas turbines. *Journal of Engineering for Gas Turbines and Power* **130**.

SMITH., G. P., M.GOLDEN, D., FRENKLACH, M., MORIARTY, N. W., EITENEER, B., GOLDENBERG, M., BOWMAN, C. T., HANSON, R. K., SONG, S., GARDINER, J. W. C., LISSIANSKI, V. V. & QUI, Z. 1999 $http://www.me.berkeley.edu/gri\_mech$.

SPALDING, D. B. 1971 Mixing and chemical reaction in steady confined turbulent flames. *Proc. Combust. Inst.* **13**, 649–657.

SPALDING, D. B. 1976 Development of the eddy-break-up model of turbulent combustion. *Proc. Combust. Inst.* **16**, 1657–1663.

WARNATZ, J., MAAS, U. & DIBBLE, R. W. 2006 *Combustion. Physical and chemical fundamentals, modeling and simulation, experiments, pollutant formation*, 4th edn. Springer.

WESTBROOK, C. K. & DRYER, F. L. 1984 Chemical kinetic modeling of hydrocarbon combustion. *Prog. Energy Combustion Sci.* **10**, 1–57.

YAKHOT, V., ORSZAG, S. A., THANGAM, S., GATSKI, T. B. & SPEZIALE, C. G. 1992 Development of turbulence models for shear flows by a double expansion technique. *Physics of Fluids A* **4**, 1510–1520.